Available online at www.sciencedirect.com
SCIENCE DIRECT®
ELSEVIER
European Journal of Mechanics B/Fluids 23 (2004) 51–63
EUROPEAN JOURNAL OF MECHANICS B/FLUIDS

Numerical simulations of VIV on long flexible cylinders immersed in complex flow fields

Julio Romano Meneghini [a,*], Fábio Saltara [a], Rodrigo de Andrade Fregonesi [b], Cássio Takeshi Yamamoto [b], Enrique Casaprima [c], José Alfredo Ferrari Jr. [d]

[a] *Department of Mechanical Engineering, EPUSP – University of São Paulo, av. Prof. Mello de Moraes, 2231, CEP 05508-900 São Paulo, SP, Brazil*
[b] *Department of Naval Engineering, University of São Paulo, Brazil*
[c] *CENPES, Rio de Janeiro, Brazil*
[d] *E&P, Petrobras, Rio de Janeiro, Brazil*

Received 29 March 2003; received in revised form 15 September 2003; accepted 15 September 2003

Abstract

The main purpose of this paper is to investigate the hydroelastic interactions that take place between long oscillating flexible cylinders and fluid forces. The cylinders are subjected to currents and shear flow emulating complex flow fields, which are present in oceanographic conditions in deep waters. In our calculations, the hydrodynamic forces are estimated by a computationally efficient discrete vortex method (DVM). The calculations are compared with results obtained employing the quasi-steady theory. The reduced velocity vs. non-dimensional amplitude curve obtained in the calculations is compared with experiments. Visualizations of the wake indicate a hybrid mode of vortex shedding along the span. Employing the terminology suggested by Williamson and Roshko [J. Fluids Struct. 2 (1988) 355], a $2S$ mode is found in regions of low amplitudes, changing to a $2P$ mode in regions of larger amplitudes. The position of the transition of modes varies with the reduced velocity.

Keywords: Vortex-induced vibration; Oscillating circular cylinder; Bluff body flow

1. Introduction

In recent years, the need to improve our knowledge on vortex-induced vibration (VIV) has greatly risen due to some challenging engineering problems. One of those is present in the field of deep-water oil extraction. Recently, offshore oil platforms have been installed in water depths of over 2000 m. Flexible pipes named risers are used to link the seabed to the offshore platform for oil production. Risers are long flexible circular cylinders exposed to all sort of oceanographic conditions. These cylinders are subjected to shear and oscillatory flows due to currents and waves, flows with a very high degree of complexity, with intensity and direction that change according to water depth. In such conditions, a better comprehension of the vortex dynamics causing vibration and fatigue of risers is essential. We believe that the main contribution of this study is to integrate known methods in an innovative way. Building a practical CFD tool to investigate the hydroelastic problems presented in this paper is of great practical interest. The life span of marine risers is significantly affected by vortex-induced vibration. The results obtained here show the expected behaviour of a long riser immersed in a uniform current and a very good agreement with the quasi-steady theory in a shear flow case.

* Corresponding author.
E-mail address: jmeneg@usp.br (J.R. Meneghini).

0997-7546/$ – see front matter
doi:10.1016/j.euromechflu.2003.09.006

With risers presenting such high aspect ratios and complex flow fields around them, a complete three-dimensional simulation at realistic conditions is unfeasible. With this in mind and aiming at the hydroelastic response of the riser structure, a numerical model in a quasi three-dimensional fashion is developed and applied to investigate some complex flows.

In order to accomplish the task of integrating the hydrodynamic force calculation and the dynamic response of the cylinder, a finite element structural model based on the Euler–Bernoulli beam theory was developed. In this model, the hydrodynamic forces are evaluated in two-dimensional strips. The technique used is the *Discrete Vortex Method* (DVM), which is a Lagrangian numerical scheme to simulate an incompressible and viscous fluid flow. Some cases of vertical marine risers are presented. The results for various uniform currents acting on single, flexible cylinders, with lengths varying from 120 to 1500 m, are shown. Envelopes of maximum and minimum in-line and transverse displacements are also shown.

This paper is divided in four sections. Brief descriptions of the structural and hydrodynamic models are given in the next section. Following that explanation, calculations for a cylinder mounted on an elastic base, and a cantilever model, are carried out. They are compared with experimental results. Then, the model is applied to a marine riser case and comparisons with the quasi-steady theory are carried out in Section 3. Finally, in the last section, conclusions are drawn based on the results presented.

2. Structural and hydrodynamic models

A finite element structural model based on the Euler–Bernoulli beam theory is employed to calculate the dynamic response of the cylinder. A general equation of motion is solved through a numerical integration scheme in the time domain. This numerical structural model is based on the studies of Patel and Witz [2] and Ferrari Jr. [3]. Firstly, we find a static solution for the riser. Then, in the dynamic analysis, the stiffness matrix obtained from the static analysis is used as an average approximation. A lumped approach is employed. A mass lumped matrix is constructed and the damping matrix is evaluated in a global manner. More details can be seen in the references mentioned above.

The *Discrete Vortex Method* (DVM) is a Lagrangian numerical scheme technique for simulating two-dimensional, incompressible and viscous fluid flow. The method employs the stream function-based boundary integral method and incorporates the growing core size or core spread method in order to model the diffusion of vorticity. In the DVM the body is discretized in N_w panels, and N_w discrete vortices with circulation Γ_i are created from a certain distance of the body, one for each panel. These vortices are convected and their velocities are assessed through the sum of the free stream velocity and the induced velocity from the other vortices. The induced velocities are calculated through the Biot–Savart law. Forces on the body are calculated integrating the pressures and viscous stresses. Viscous stresses are evaluated from the velocities in the near-wall region, and the pressure distribution is calculated relating the vorticity flux on the wall to the generation of circulation. Details about the employed method can be found in [4].

3. Calculations

3.1. Numerical evaluation of the DVM: a circular cylinder mounted on an elastic base

We carried out simulations for fixed cylinders in order to validate the vortex method. For modelling viscous diffusion, we employed the random walk technique and the core spreading method. Both methodologies yielded similar results. A non-dimensional time step $U\Delta t/D = 0.05$ was used, and 128 equal panels were employed on the cylinder surface. Vortices were created at a distance $\sigma = \Delta s/(2\pi)$ from the wall, where Δs is the length of the panel, and this distance was assigned as the core of the newly created vortices. The simulations for $Re = 10\,000$, employing the random walk technique, can be seen in Figs. 1 and 2. The obtained mean C_d is 1.20, and the Strouhal number $St = 0.19$. They are very close to the experimental values found by Roshko [5]: $C_d = 1.10$ and $St = 0.20$. In the computations slightly higher values of C_d are expected (Sarpkaya [6]) because the actual flow at $Re = 10\,000$ is three-dimensional. However, the 3D effects observed in the wake for Re higher than 200 are not an obstacle for simulations of the flow around oscillating cylinders, because high amplitude oscillations increase the spanwise correlation of the wake (Bearman [7]).

A comparison between our two-dimensional calculations, and experiments carried out by Blackburn et al. [8], are show in Fig. 3. The cylinder is mounted on an elastic basis, and the mass and damping parameters are $m^* = 4m/\rho\pi D^2 = 50.8$, $m^*\zeta = 0.122$. In these expressions, m is the mass per unit length of the oscillating system, D is the cylinder diameter, and ζ is the fraction of the critical damping. Amplitude of vibration is calculated through analogy with a sinusoidal wave: the *rms* value of the y position of the cylinder is multiplied by $\sqrt{2}$. In the experiments, the maximum amplitude is $A/D \cong 0.6$. When the reduced velocity is increased in very small steps, our calculations with the DVM reproduce the experimental results in almost all range of V_r. The maximum amplitude and the branch, in which the amplitude of oscillation is high for a range of reduced velocity, are reproduced in the calculations.

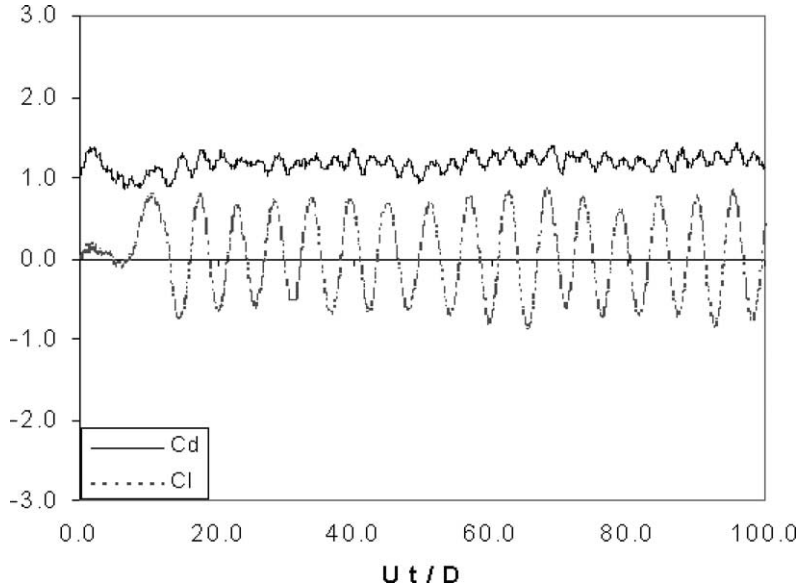

Fig. 1. Time history of drag coefficient C_d and lift coefficient C_l for the flow around a fixed cylinder, $Re = 10\,000$.

Fig. 2. Wake visualization, fixed cylinder, $Re = 10\,000$.

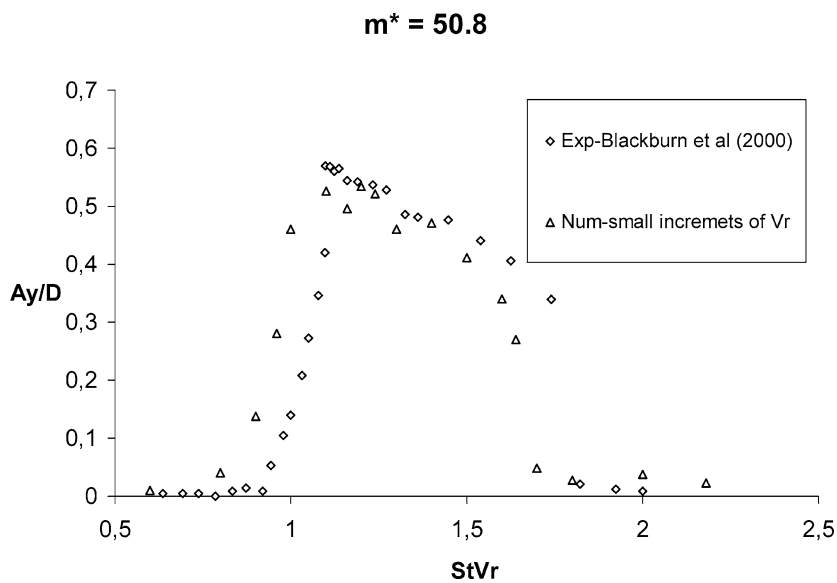

Fig. 3. Amplitude of vibration as a function of $St * V_r$ comparisons between simulations with DVM, and experimental results from [9]. In all cases $m^* = 50.8$.

Simulations of a cylinder mounted on an elastic basis for $m^* = 3.3$, $m^*\zeta = 0.013$, and $Re = 10\,000$, are shown in Fig. 4. Our simulations are compared to the experimental results obtained by Khalak and Williamson [9]. The simulations for the free-vibrating cylinder were carried out for a range of reduced velocity V_r between 2 and 16. Amplitude of vibration results are plotted as a function of the reduced velocity in Fig. 4, along with the experimental results from [9]. Wakes visualized for velocities $V_r = 2.0$, 7.5, and 10 can be seen in Figs. 5–7. We can observe, based on the analyses of Fig. 4, that for this case the maximum amplitude in our simulations occurs for $V_r = 7.5$, and is about $A/D \cong 0.65$, well below the maximum amplitude $A/D = 1.08$ for $V_r = 5.8$ found in [9]. Apparently, only the high amplitude mode for $5.00 < V_r < 7.00$ is not observed in our calculations. There is a very good agreement in the region of the lower amplitude mode of vibration. Results for $V_r < 5.00$ and $7.00 < V_r < 10.00$ are in a reasonable agreement with experiments.

Our simulations for the cylinder mounted on an elastic base give excellent results for a mass parameter $m^* \cong 50$. For mass parameter values below 10, the simulations with the DVM or higher order methods give good results for the lower branch only. They still fail to capture the peak observed in experiments. In a simulation of a very long cylinder immersed in a shear flow, only a very small portion of the body, if any, will be subjected to the reduced velocity for which the amplitude reaches a peak.

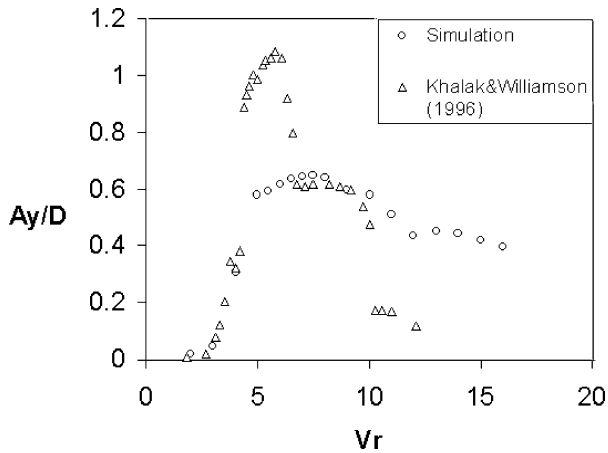

Fig. 4. Amplitude of vibration as a function of the reduced velocity. Experimental results from [9], $m^* = 3.3$.

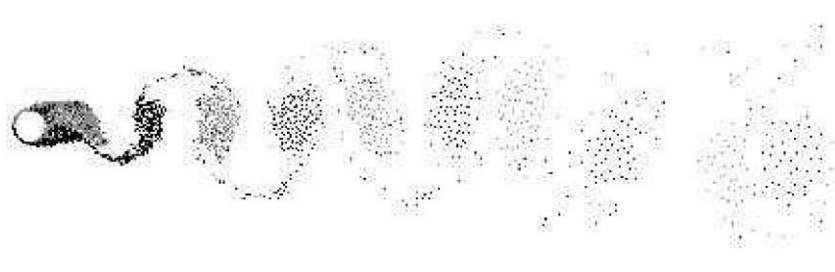

Fig. 5. Wake visualization, $V_r = 2.00$.

Fig. 6. Wake visualization, $V_r = 7.50$.

Fig. 7. Wake visualization, $V_r = 10.00$.

In such a case, the error in predicting the amplitude will be restricted to a small portion of the cylinder, and probably the overall effect will be small.

The results presented here give a very good reason for choosing the DVM for simulations with long cylinders ($L/D \approx 2000$–8000). The DVM simulations proved to be inexpensive when compared with higher order and more accurate methods. A typical run, with 1000 time steps and $U\Delta t/D = 0.05$, took around 22 min in an AlphaServer DS20E workstation with a dual EV67 Alpha processor, and 2 MB of RAM. The same run took around two minutes in a cluster with 64 Pentium IV processors.

3.2. Results for the cantilever cylinder model, $L/D = 94.50$

In this section, we compare calculations employing the code briefly described in Section 2 with experiments by Fujarra [10] and Fujarra et al. [11]. They studied the amplitudes of vibrations due to vortex induced vibration in a cantilever cylinder, and obtained the non-dimensional amplitude vs. reduced velocity curve. The numerical simulations employing the DVM are carried out in order to reproduce their results. Before comparing the numerical simulations with the experimental results, a set of calculations have been carried out to check the numerical resolution and convergence of the structural part of the computational code. The cantilever has been discretised in 10, 30, and 60 structural elements. The amplitudes converged for a number of elements above 30. For this reason, and with the intention of having a proper numerical accuracy, a number of 60 elements have been chosen for the simulations.

The characteristics of the cantilever cylinder can be found in [10]. The mass and damping parameters are $m^* = 2.4$, and $m^*\zeta = 0.013$, respectively. Simulations have been carried out for values of reduced velocity varying from 3.0 to 20.0 with the purpose of obtaining the response amplitudes of oscillation. These velocities correspond to Reynolds numbers, *Re*, in the range $7000 \leqslant Re \leqslant 47\,000$. The numerical and experimental results are compared in Fig. 8. The cantilever amplitudes are normalized

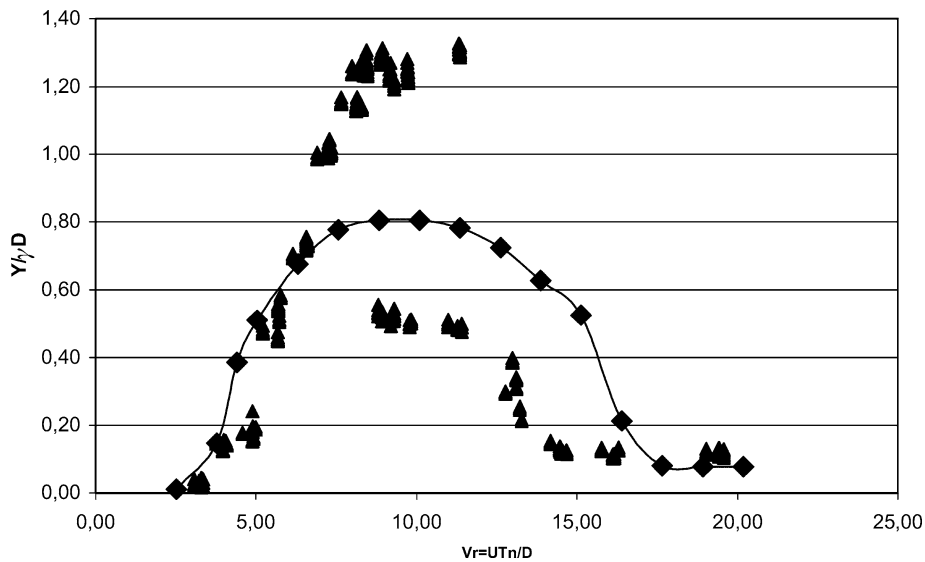

Fig. 8. Comparison of numerical calculations (—♦—), and experimental results obtained by Fujara [10] of an oscillating cantilever cylinder (▲).

using an eigenmode factor γ, as explained in [11]. The structure vibrates in the first mode for all reduced velocities. In this case, $\gamma = 1.305$, and the normalised amplitude is $Y/\gamma D$. The reduced velocity is defined with this mode period. As it can be observed, a very good agreement is obtained in part of the lock-in region. In the region of maximum amplitude our calculations yield amplitude between the upper and lower branch. The maximum non-dimensional amplitude value reached is about 0.8. Figure 9 shows a wake visualization of the flow at the reduced velocity $V_r = 5$. The strips are plotted separately, and the

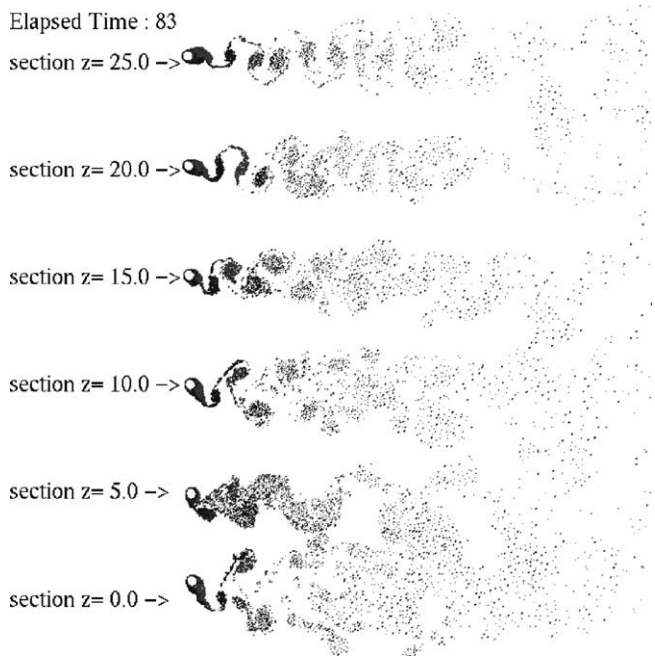

Fig. 9. Wake visualization for $V_r = 5.0$: $z/D = 0$ is the bottom section, and $z/D = 25$ is the top of the cylinder.

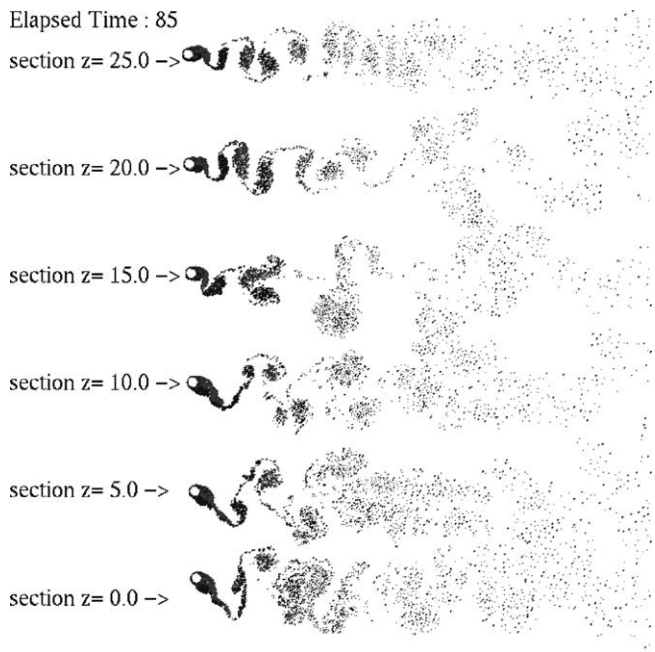

Fig. 10. Wake visualization for $V_r = 9$. $z = z_{\text{section}}/D = 0$ is the free end of the cylinder; $z = z_{\text{section}}/D = 25.0$ is close to the fixed end of the cylinder.

position is normalized by the cylinder diameter ($z = z_{\text{section}}/D$). Section $z = 0$ corresponds to the free end of the cylinder, i.e. the bottom strip; z increases upward. The section $z = 25$ is close to the fixed end of the cylinder. In Fig. 9, we can observe a hybrid mode close to the free end. There is a transition from a $2S$ mode close to the top to a $2P$ mode occurring around section $z = 5$. Figure 10 shows the wake visualization of the flow for reduced velocity $V_r = 9$. It can be seen that in this case there is a transition from a $2S$ mode close to the top to a $2P$ mode near the bottom. We can also observe that there is a dependency of this transition point with the reduced velocity. At $V_r = 9$, the transition occurs at section $z = 15$.

It is interesting to compare these results with those by Techet et al. [12]. They studied experimentally the flow around a tapered cylinder. The experiments were taken at different reduced velocities, Reynolds numbers and average diameters. In some cases, a hybrid mode was observed. A $2S$ pattern along the region that experienced lower amplitudes, and a $2P$ pattern along the region that experienced greater amplitudes, were observed. The location of the transition was stable and repetitive when the same experiment was carried out. It was observed that in the region of the transition of modes, $2S$ to $2P$, the two patterns were phase locked and had the same frequency; there were no jumps in the phase angle inside this region.

3.3. Results for a marine riser with $L/D \cong 480$

Some results of a marine riser simulation are presented in this section. The riser has the following characteristics: water depth = 100 m, riser length = 120 m, riser external diameter = 0.25 m, riser pipe inside diameter = 0.2116 m, top tension TTOP = 200 kN (∼1.5 times the riser self-weight), modulus of elasticity of riser pipe 2.10×10^8 kN·m^{-2}, specific weight of the fluid surrounding the riser bore 1025 kg·m^{-3}, specific weight of the fluid in the riser bore 800 kg·m^{-3}, specific weight of the riser wall material 7700 kg·m^{-3}. The mass and damping parameters are $m^* = 2.7$, and $m^*\zeta = 0.054$ for this case.

The riser is modelled with 80 elements equally spaced below the water level (80 hydrodynamic sections) and 20 elements equally spaced above it. The riser is subjected to uniform flow, simulations were carried out at current velocities $U = 0.23$, 0.38, 0.54, and 0.85 m/s, which correspond to a Reynolds number in the range $5.8 \times 10^4 < Re < 2 \times 10^5$. The envelopes of maximum and minimum displacements transverse to the direction of the flow are shown in Figs. 11–14. The reduced velocity V_r is defined with the natural frequency of the oscillating mode. The reduced frequency is $f_r = 1/V_r$. In Table 1, the current velocity, vibration mode, and reduced velocity and frequencies are shown. Analyzing the results shown in Fig. 11, one can clearly see that the structure vibrates in the first mode. Increasing the velocity to $U = 0.38$ m/s, there is a change of oscillation mode, and the riser starts vibrating predominantly in the second mode, as can be seen in Fig. 12. For velocities $0.54 \leqslant U \leqslant 0.78$ m/s, the risers oscillates mainly in the third mode, as shown in Fig. 13. When the velocity is in the range $0.86 \leqslant U \leqslant 0.93$ m/s, the vibration occurs mostly in the fourth mode, as shown in Fig. 14. We can observe in Figs. 12–14 that the response is not a single mode since there is no zero response at nodes. Apparently, for this reason, this cannot be a standing wave oscillation. Analysing the amplitude envelopes shown in those figures, one can see that maximum amplitude reached in the calculations is around $A/D \cong 0.60$. One can notice examining Table 1 that there is a change in the vibration mode as we increase the current speed and the reduced velocity approaches $V_r = 6.0$. The oscillation mode selection occurs in order to keep the reduced velocity in the range $4 \leqslant V_r \leqslant 6.5$. If we suppose that the dimensionless frequency is approximately 0.2, and also knowing the diameter of the riser and the velocity of the current, we can estimate the expected excitation frequency and consequently the mode that the structure will predominantly vibrate.

Now, the results obtained by the CFD model are compared with those from calculations employing the quasi-steady theory as described by Ferrari Jr. [3]. In this reference, a more conventional approach to the hydrodynamic force estimation was employed. In his work, the Morison´s equation is utilized to obtain the in-line hydrodynamic force. The quasi-steady theory is employed to find the transverse force. More details of his procedure can be found in [13,3].

The quasi-steady model cannot be applied to the uniform current case since it does not capture the synchronization between the forces and displacements. In the presence of a shear flow, multiple frequencies of vortex shedding take place and a single structural mode does not control the shedding process. With this in mind, our comparisons are carried out only for a shear flow case.

Table 1
Current velocity, vibration mode, and reduced velocity and frequency

U (m/s)	Mode	V_r	f_r	U (m/s)	Mode	V_r	f_r
0.16	1st	4.51	0.22	0.54	3rd	4.00	0.25
0.23	1st	6.76	0.15	0.62	3rd	4.57	0.22
0.31	2nd	4.00	0.25	0.70	3rd	5.15	0.19
0.39	2nd	5.00	0.20	0.78	3rd	5.72	0.17
0.40	2nd	5.14	0.20	0.86	4th	4.03	0.25
0.47	2nd	6.00	0.17	0.93	4th	4.40	0.23

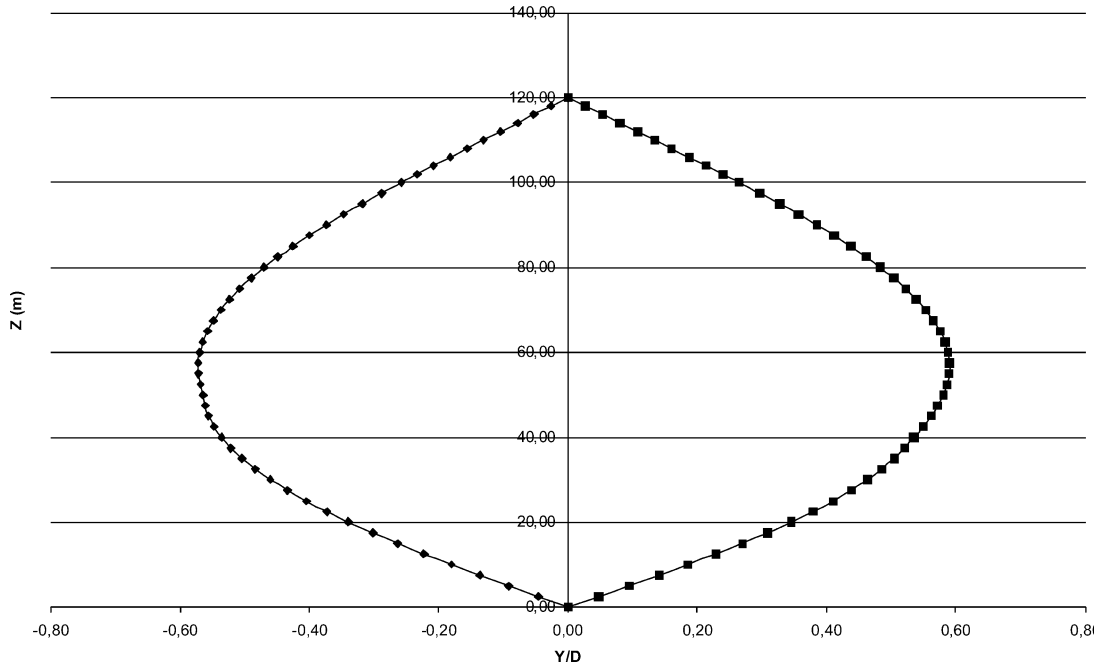

Fig. 11. Transverse envelope, maximum and minimum transverse displacements, $U = 0.23$ m/s.

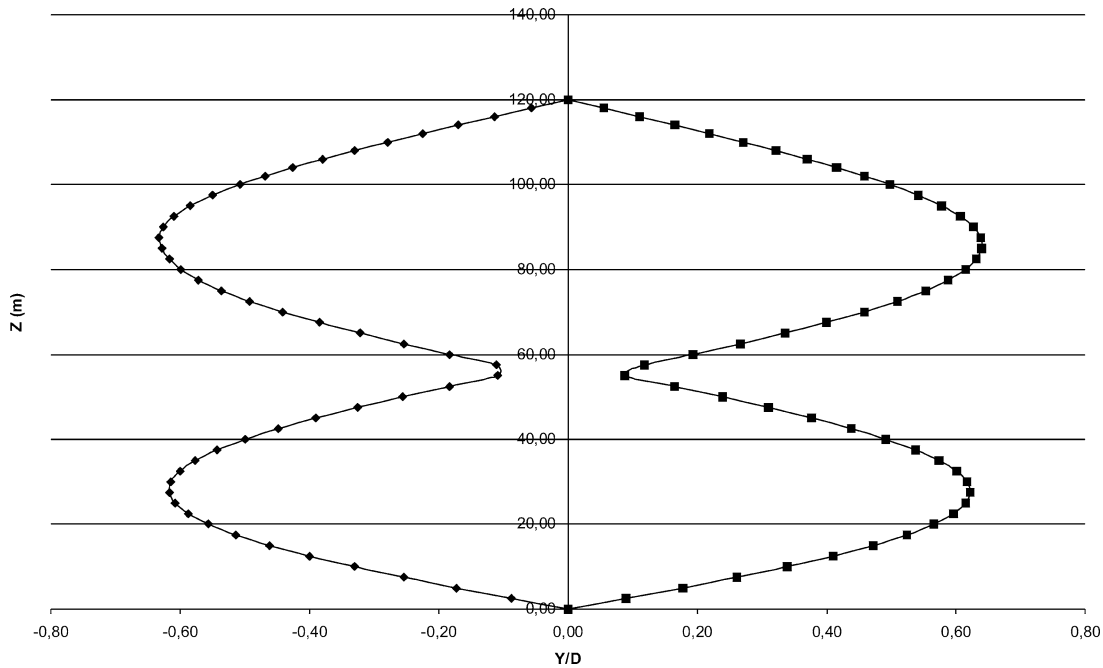

Fig. 12. Transverse envelope, maximum and minimum transverse displacements, $U = 0.38$ m/s.

Two cases are chosen. In both, the current varies linearly along the span. The structural characteristics of the riser are the same as in the previous case. The input parameters employed in the quasi-steady theory calculations are the same as those employed by Ferrari Jr. [3]: drag coefficient $C_d = 1.2$, added mass coefficient $C_A = 0.6$, shedding phase $\varphi = 20°$, Strouhal number $St = 0.2$, and transverse force amplitude $C_t = 1.2$. The riser is modelled with 40 elements equally spaced below the water level and 10 elements, also equally spaced, above the water level. The time step is $\Delta t = 0.05$. The dominant modes are:

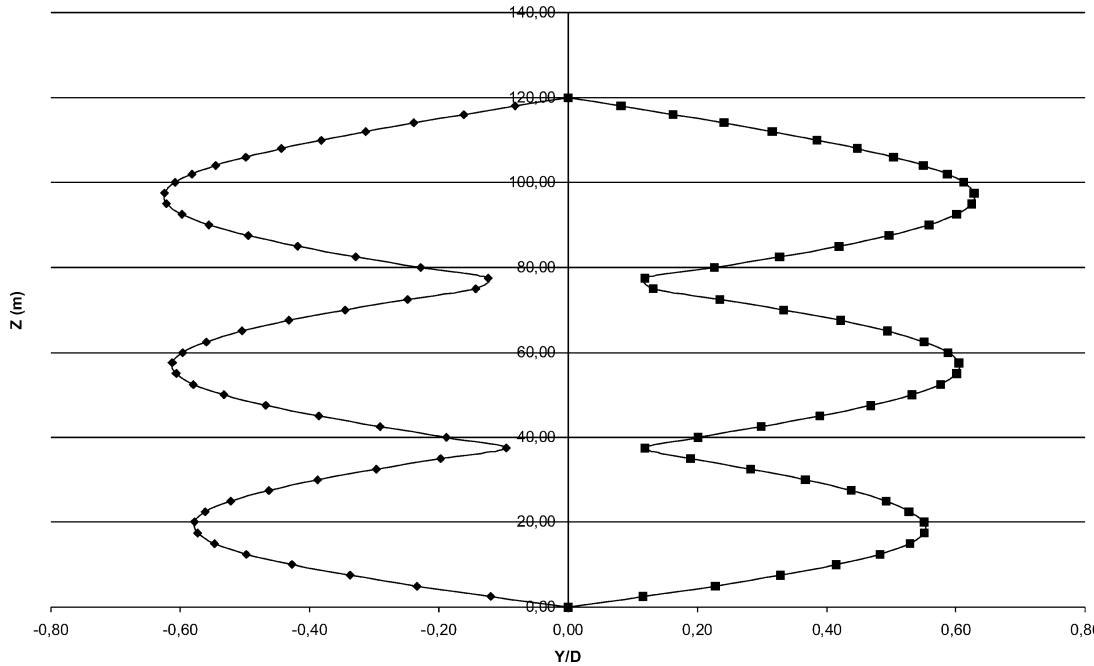

Fig. 13. Transverse envelope, maximum and minimum transverse displacements, $U = 0.54$ m/s.

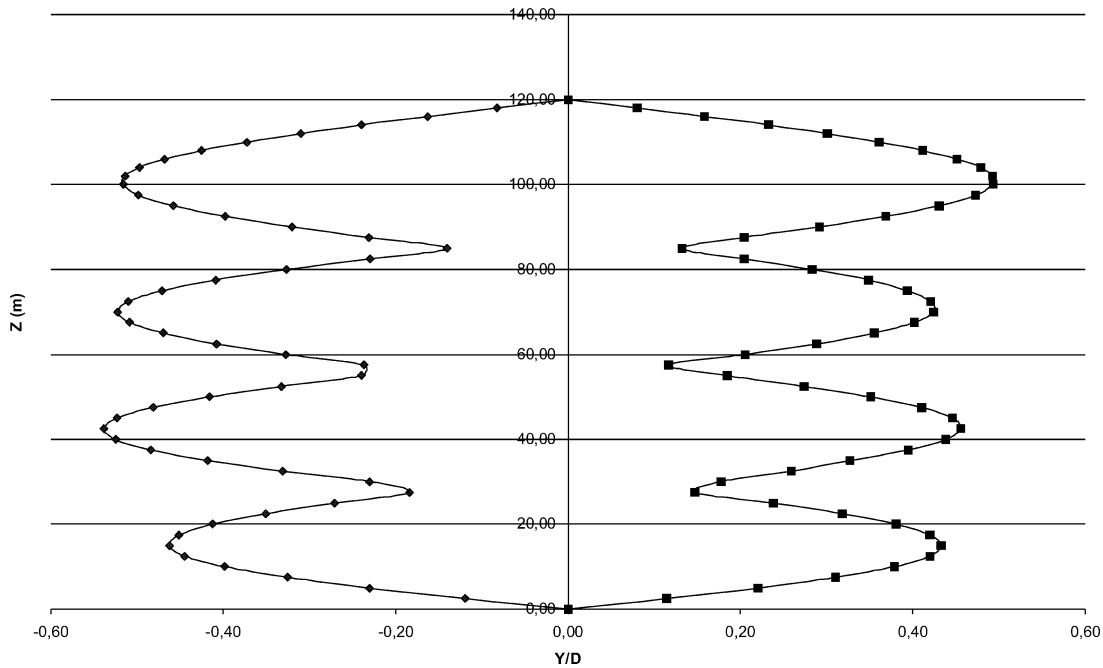

Fig. 14. Transverse envelope, maximum and minimum transverse displacements, $U = 0.85$ m/s.

the first and second in the in-line direction with damping factor $\zeta = 2\%$; the fourth and fifth in the transverse direction with damping factor $\zeta = 2\%$. The two shear flow considered for our comparisons vary linearly. In the first case, a trapezoidal current profile is adopted. The fluid velocity varies from 0.4 m/s at the sea bed to 1.2 m/s at the water level. In the second case a triangular profile is adopted. The velocity at the seabed is 0.4 m/s, at the middle of the riser is 1.2 m/s, and at the water level is 0.4 m/s illustrates both cases.

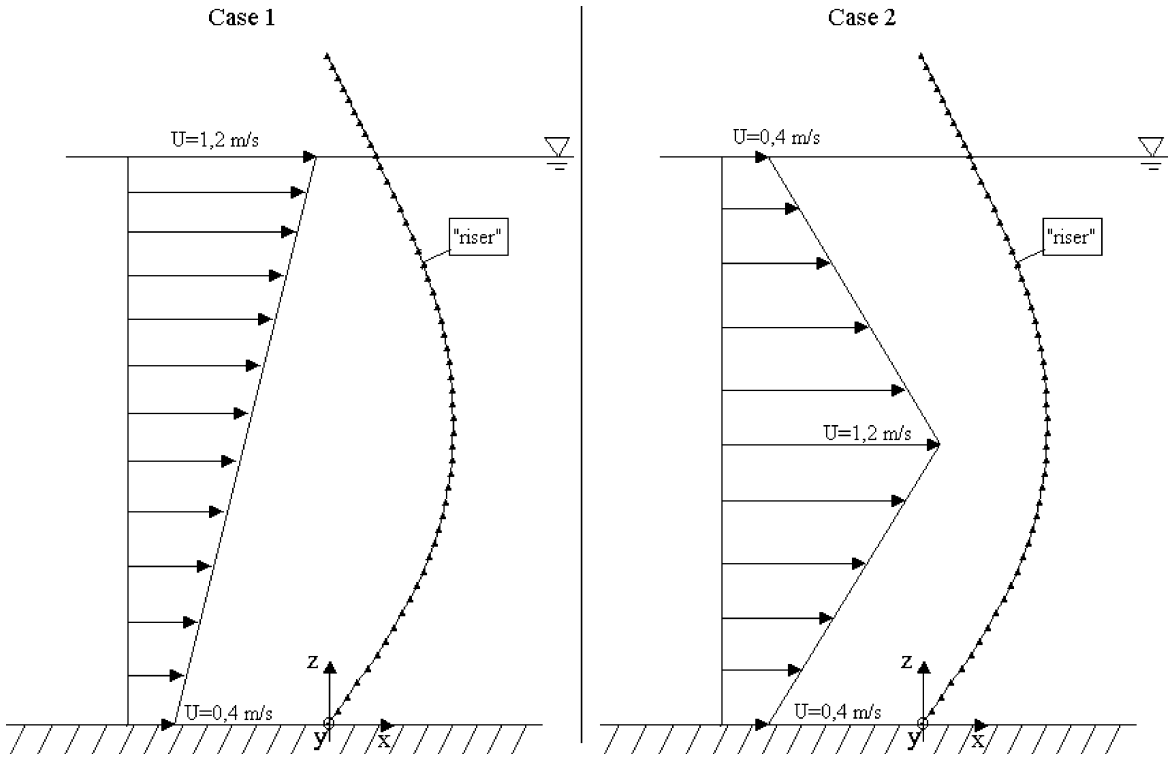

Fig. 15. Shear flow, Cases 1 and 2.

The maximum and minimum envelopes in the transverse direction are shown in Figs. 16 and 17. Comparing the transverse envelope obtained with the DVM and quasi-steady theory, one can notice that the envelopes have very similar shapes. We observe that the dominant mode is the fourth one. However, if we observe the structural displacement time history, we can observe a slight difference in the results. The signal obtained with the quasi-steady theory has a beating behaviour. On the other hand, the transverse displacements obtained by the DVM present a much less intense beating.

The amplitude results obtained with the quasi-steady theory have very small oscillation amplitudes in some particular instants of time. When the oscillation amplitude increases, we notice that the structure vibration changes from the first to the fourth mode. In the results obtained with the DVM, we observed vibration changing from the second to the fourth mode. However, these modes appear during smaller periods of time than those observed with the quasi-steady theory. A possible reason for this difference may be due to the phase of the transverse force, which, in the quasi-steady model, is considered constant along the cylinder span.

3.4. Results for a marine riser with $L/D \cong 4600$

In this section, numerical applications based on the method described above for realistic offshore conditions are presented. The base case definition can be found in [14].The input data specifications for these calculations are as follows: riser length = 1500 m, water depth = 1500 m, a top tensioned riser is considered with top tension TTOP = 3390.7 kN, external diameter = 0.3239 m, riser internal diameter = 0.2889 m, sectional inertia = 1.9833×10^{-4} m^4, modulus of elasticity of the pipe = 2.07×10^{11} N·m^{-2}, pipe density = 7850 kg·m^{-3}, internal fluid density = 800 kg·m^{-3}, water density = 1025 kg·m^{-3}, mass per unit length = 184.68 kg·m^{-1} and submerged weight per unit length = 982.82 N·m^{-1}. The mass and damping parameters are $m^* = 1.41$ and $m^*\zeta = 0.028$.

A discretization of the riser into 600 elements below the still water level is used. The offshore riser is subjected to current flow only, i.e. no wave is present. The velocity profiles are defined in terms of the reference velocity V_0. The following value of V_0 is presented in this paper: $V_0 = 1.10$ m/s, which correspond to synchronisation of the 20th mode. The velocity profile considered has an uniform velocity V_0 for $0 \leqslant z/L \leqslant 0.75$, then a linear profile ranging from V_0 at $z/L = 0.75$ to $2V_0$ at $z/L = 1$ as shown in Fig. 18. The envelope of transverse response experienced by the riser can be seen in Fig. 19. This figure shows that the maximum amplitude is around $A/D = 0.9$.

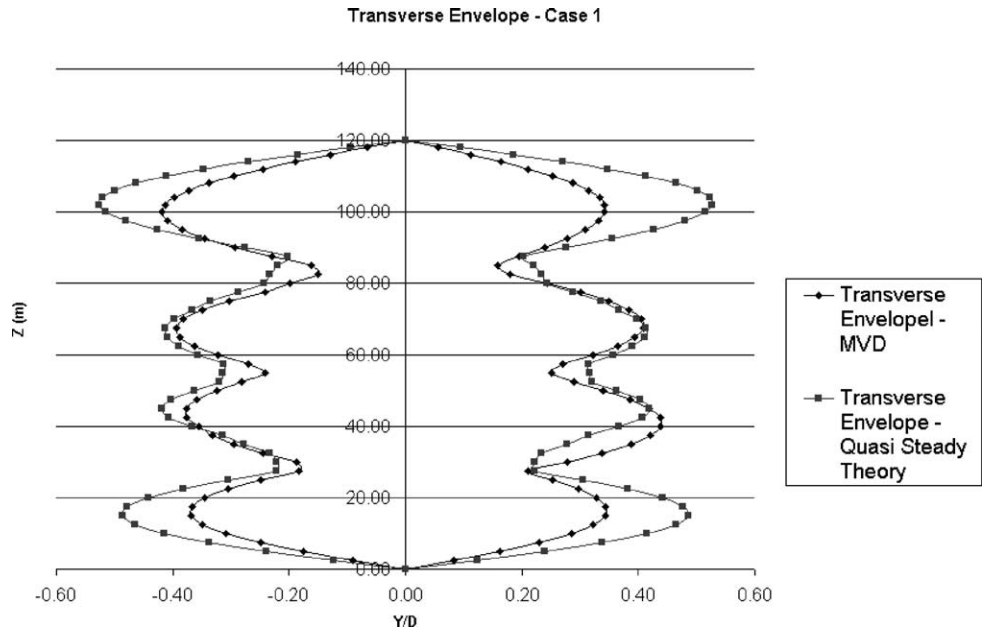

Fig. 16. Transverse envelope (Case 1), comparison between CFD predictions and quasi-steady calculations.

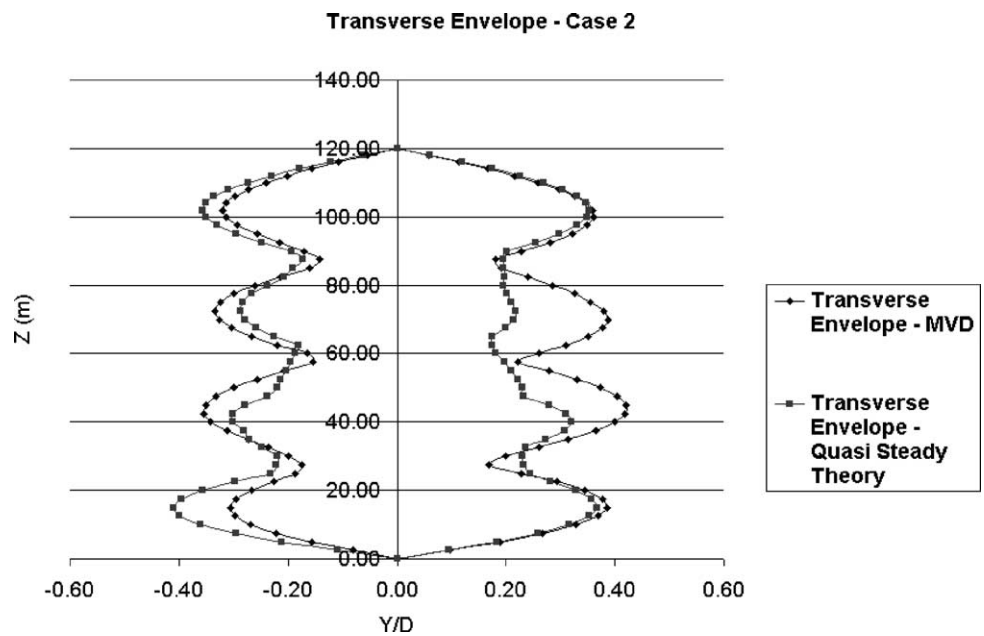

Fig. 17. Transverse envelope (Case 2), comparison between CFD predictions and quasi-steady calculations.

4. Conclusions

Some results of calculations of circular cylinders subjected to VIV were shown in this paper. The numerical results for an oscillating cylinder mounted on a elastic base, with a mass parameter $m^* = 50.8$, compare very well with experiments. However, for a lower mass parameter $m^* = 3.3$, the upper branch related to the maximum amplitude of oscillation observed in the experiments is not captured in our calculations. For the cantilever model, the general trend of the amplitude vs. reduced velocity curve obtained here compares well with the experiments. The only disagreement is again related to the maximum amplitude of oscillation: the calculations yield a lower value than the experimental result. The reason for this disagreement is

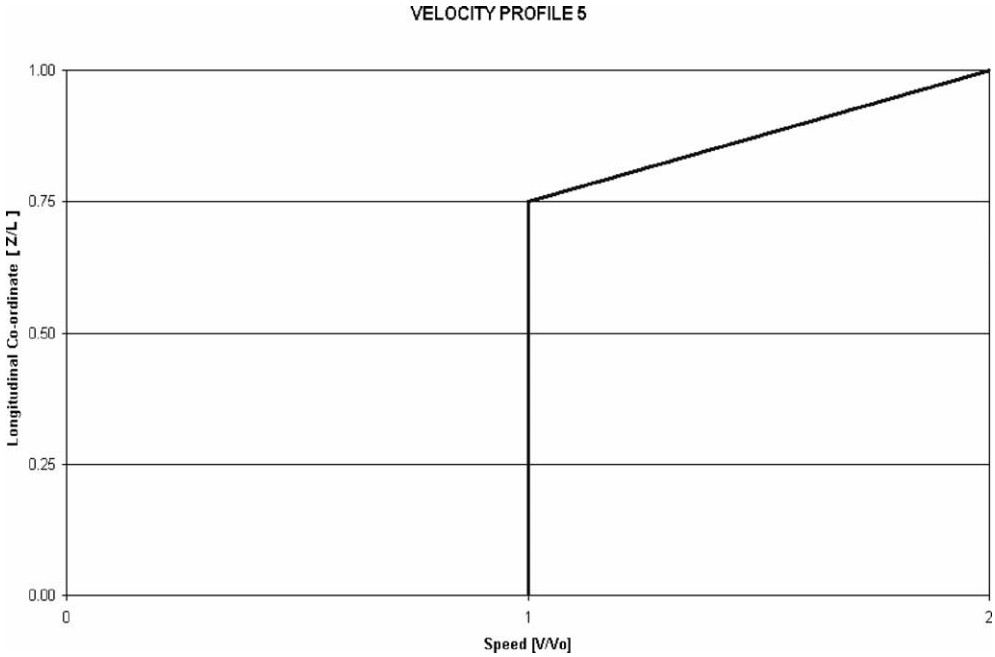

Fig. 18. Shear flow, Case 3.

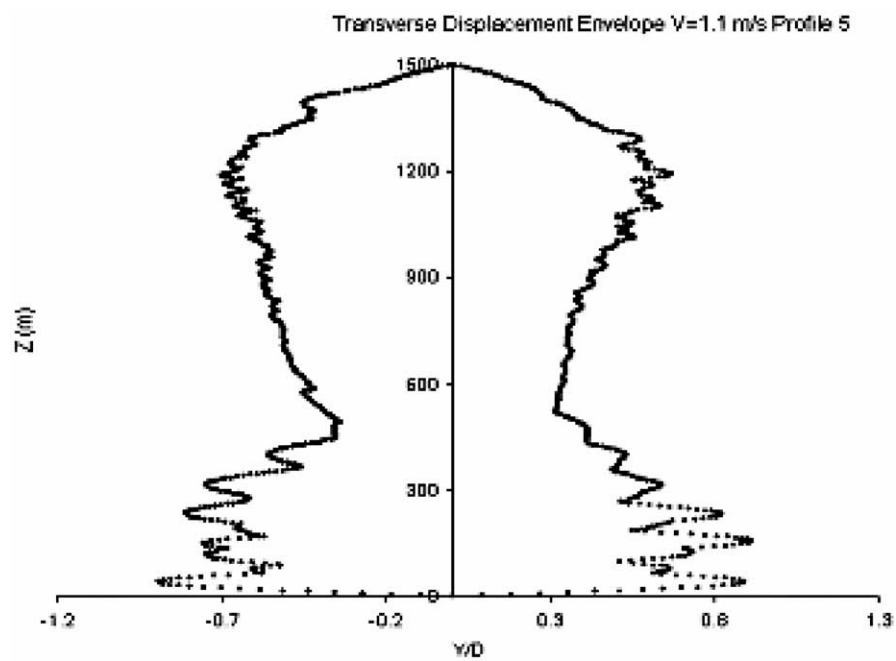

Fig. 19. Transverse envelope (Case 3), comparison between CFD predictions and quasi-steady calculations.

under investigation and will be addressed in a forthcoming paper. Single riser simulations provided expected vibrating modes and the comparisons with the quasi-steady theory give a very good agreement. The main feature of the procedure adopted in this paper is the use of a Lagrangian scheme for the calculation of hydrodynamic force and a three-dimensional scheme for the structural response evaluation. With such an approach, we are able to simulate multiple risers with no need for mesh interpolations at every time step. We would like to emphasize that with this work we did not intend to develop a new method.

The objective was to integrate a known structural model with the DVM. Doing so, a computationally efficient and practical tool to study the flow around very long marine risers is developed and validated.

Acknowledgements

The authors are grateful to FINEP, CNPq, FAPESP, and PETROBRAS (The Brazilian State Oil Company) for providing them a research grant for this project. The authors also acknowledge José A.P. Aranha, Clóvis A. Martins, Celso P. Pesce, and André L.C. Fujarra for their useful comments regarding our numerical simulations.

References

[1] C.H.K. Williamson, A. Roshko, Vortex formation in the wake of an oscillating cylinder, J. Fluids Struct. 2 (1988) 355–381.
[2] M.H. Patel, J.A. Witz, Compliant Offshore Structures, Butterworth–Heinemann, England, 1991.
[3] J.A. Ferrari, Hydrodynamic loading and response of offshore risers, PhD thesis, University of London, UK, 1998.
[4] C.T. Yamamoto, R.A. Fregonesi, J.R. Meneghini, F. Saltara, J.A. Ferrari, Numerical simulations of vortex-induced vibration of flexible cylinders, J. Fluids Struct. (2002), submitted for publication.
[5] A. Roshko, Experiments on the flow past a circular cylinder at very high Reynolds numbers, J. Fluid Mech. 10 (1961) 354.
[6] T. Sarpkaya, Computational methods with vortices—The 1988 Freeman Scholar lecture, J. Fluids Eng. 111 (1989) 5–52.
[7] P.W. Bearman, Vortex shedding from oscillating bluff bodies, Ann. Rev. Fluid Mech. 16 (1984) 195–222.
[8] H.M. Blackburn, R.N. Govardhan, C.H.K. Williamson, A complementary numerical and physical investigation of vortex-induced vibration, J. Fluids Struct. 15 (2000) 481–488.
[9] A. Khalak, C.H.K. Williamson, Dynamics of a hydroelastic cylinder with very low mass damping, J. Fluids Struct. 10 (1996) 455–472.
[10] A.L.C. Fujarra, Estudo em Modelo Reduzido de Tubo, Flexível e Liso, Submetido ao Fenômeno de Vibração Induzida pela Vorticidade, MSc thesis, Universidade de São Paulo, 1997.
[11] A.L.C. Fujarra, C.P. Pesce, F. Flemming, C.H.K. Williamoson, Vortex-induced vibration of a flexible cantilever, J. Fluids Struct. 15 (2001) 651–658.
[12] A.H. Techet, F.S. Hover, M.S. Triantafylou, Vortical patterns behind a tapered cylinder oscillating transversely to a uniform flow, J. Fluids Mech. 363 (1998) 79–96.
[13] P.W. Bearman, J.M.R. Graham, E.D. Obasaju, A model equation for the transverse forces on cylinders in oscillating flows, Appl. Ocean Res. 6 (3) (1984) 166–172.
[14] Stride JIP (Steel Risers for Deepwater Environments), VIV Consultants Forum, Base Case Definition Doc. 1500-RPT-002, 2H Offshore Engineering Ltd.